

Optical probe on doping modulation of magnetic Weyl semimetal $\text{Co}_3\text{Sn}_2\text{S}_2$

L. Wang,^{1,*} S. Zhang,^{2,*} B. B. Wang,² B. X. Gao,¹ L. Y. Cao,¹
X. T. Zhang,¹ X. Y. Zhang,¹ E. K. Liu,^{2,†} and R. Y. Chen^{1,†}

¹*Center for Advanced Quantum Studies and Department of Physics,
Beijing Normal University, Beijing 100875, China*

²*State Key Laboratory for Magnetism, Institute of Physics,
Chinese Academy of Sciences, Beijing 100190, China*

(Dated: January 9, 2024)

The magnetic Weyl semimetal $\text{Co}_3\text{Sn}_2\text{S}_2$ is extensively investigated due to its giant anomalous Hall effect (AHE). Recent studies demonstrate that the AHE can be effectively tuned by multi-electron Ni doping. To reveal the underlying mechanism of this significant manipulation, it is crucial to explore the band structure modification caused by Ni doping. Here, we study the electro-dynamics of both pristine and Ni-doped $\text{Co}_{3-x}\text{Ni}_x\text{Sn}_2\text{S}_2$ with $x = 0, 0.11$ and 0.17 by infrared spectroscopy. We find that the inverted energy gap around the Fermi level (E_F) gets smaller at $x = 0.11$, which is supposed to enhance the Berry curvature and therefore increase the AHE. Then E_F moves out of this gap at $x = 0.17$. Additionally, the low temperature carrier density is demonstrated to increase monotonically upon doping, which is different from previous Hall measurement results. We also observe the evidences of band broadening and exotic changes of high-energy interband transitions caused by doping. Our results provide detailed information about the band structure of $\text{Co}_{3-x}\text{Ni}_x\text{Sn}_2\text{S}_2$ at different doping levels, which will help to guide further studies on the chemical tuning of AHE.

INTRODUCTION

The anomalous Hall effect (AHE) was initially discovered in ferromagnetic materials with a magnitude proportional to the magnetisation[1, 2]. For a very long time, AHE was considered as a unique property of time-symmetry-breaking systems with a net magnetisation, whose origination seemed too complicated to be clearly revealed. In 1980s, the development of Berry phase theory has brought a breakthrough in understanding the physical mechanism of AHE[3], which substantially advanced our perspectives of this phenomenon. Nowadays, it is generally believed that AHE can be generated from two different mechanisms: the extrinsic mechanism caused by the scattering effect (skew-scattering[4] and side-jump[5]) and the intrinsic mechanism related to Berry curvature[6, 7]. Among them, the intrinsic contribution is directly related to the topological properties of the Bloch state. Therefore, the anomalous Hall conductivity (AHC) depends only on the band structure of the ideal crystal lattice, which can be calculated directly by the Kubo formula[7–9].

A great number of materials have been reported to cast giant intrinsic AHE, such as Kagome metal Nd_3Al [10], Weyl semimetal Mn_3Sn [11], Dirac semimetal Fe_3Sn_2 [12], topological insulator MnBi_2Te_4 [13], etc. Among them, Weyl semimetals are of special interest as the Berry curvature near the Weyl points is inherently divergent, which is supposed to contribute a large AHC when they are near the Fermi surface[14–16]. Moreover, the AHC generated by the topologically protected Weyl point is rather robust to perturbations such as lattice distortion and chemical substitution[14, 17], which is a vital advan-

tage for developing next-generation spintronic devices.

$\text{Co}_3\text{Sn}_2\text{S}_2$ is a typical magnetic Weyl semimetal with an AHC up to $\sim 1130 \text{ } \Omega^{-1}\text{cm}^{-1}$ and anomalous Hall Angle of $\sim 20\%$. Previous studies have shown that its large AHE is dominated by the divergent Berry curvature near the Weyl point at $\sim 60 \text{ meV}$ above the Fermi level (E_F)[18, 19]. Subsequently, attempts were made to modulate the AHC of the material by doping holes or electrons in order to fine-tune the relative position of the E_F and the Weyl point[20–24]. Thereinto, Shen *et al.* have succeeded in elevating the AHC of $\text{Co}_3\text{Sn}_2\text{S}_2$ by multi-electron Ni doping, which reaches a maximum in $\text{Co}_{3-x}\text{Ni}_x\text{Sn}_2\text{S}_2$ when $x = 0.11$ ($\sim 1380 \text{ } \Omega^{-1}\text{cm}^{-1}$). It is suggested by the authors that this abnormal enhancement is mainly generated by intrinsic contributions, due to the modulated electronic structure by the local disorder effect of the doped atoms, based on theoretical calculations[20]. Therefore, it will be very illuminating to investigate what really happens to the electron band structure of $\text{Co}_3\text{Sn}_2\text{S}_2$ when doped with Ni. Lohani *et al.* have performed angle-resolved photoemission spectroscopy (ARPES) measurements on the significantly doped $\text{Co}_{3-x}\text{Ni}_x\text{Sn}_2\text{S}_2$ with $x = 0.6$, which reveals the shift of several bands compared to the pristine compound, and the emergence of an extra electron pocket near E_F that is occupied by added electrons.[25].

Here, we study the band structure evolution of $\text{Co}_{3-x}\text{Ni}_x\text{Sn}_2\text{S}_2$ with $x = 0, 0.11$ and 0.17 at different temperatures by infrared spectroscopy, which is another important technique to explore the band structure near the E_F [26]. We find that the interband transition peak associated with the inverted energy gap near the Weyl points shows a red shift with a small amount of Ni dop-

ing, but disappears completely with an excessive amount of Ni doping. This is consistent with the theoretical calculation of previous report, and possibly responsible for the significant enhancement of the AHE. We also observe that the total plasma frequency increases significantly with the increase of Ni concentration, which is different with the results of Hall measurement[20]. Our work provides detailed information towards revealing the underlying mechanism of the tuning of AHE by chemical doping.

EXPERIMENTAL TECHNIQUES

Three $\text{Co}_{3-x}\text{Ni}_x\text{Sn}_2\text{S}_2$ single crystals with nominal concentrations of $x = 0, 0.11$ and 0.17 were synthesized by the method of Sn and Pb mixed flux growth[20]. Infrared spectroscopic studies were performed with the Fourier transform infrared spectrometer Bruker 80V in the frequency range from 50 to 40 000 cm^{-1} over three samples growing shiny surfaces. As for the measurement of the frequency dependent reflectivity $R(\omega)$, in-situ gold and aluminum overcoating techniques were employed to eliminate the effect of microscopic surface texture of single crystal compounds to obtain the absolute value of reflectivity[27]. The real part of the optical conductivity $\sigma_1(\omega)$ is derived from the Kramers-Kronig transformation of the reflectivity $R(\omega)$, which is extrapolated to zero at the low frequency by the Hagen-Rubens relation and to high frequency by the x-ray atomic scattering function[28]. Since the experimental data of the reflectivity spectra were measured up to 40 000 cm^{-1} in the ultraviolet region, the high frequency extrapolation has little influence on the low frequency behaviour of the real part of conductivity via Kramers-Kronig transformation.

RESULTS AND DISCUSSION

The reflectivity $R(\omega)$ and the real part of optical conductivity spectra $\sigma_1(\omega)$ of $\text{Co}_{3-x}\text{Ni}_x\text{Sn}_2\text{S}_2$ ($x = 0, 0.11$ and 0.17) measured at different temperatures are shown in Fig. 1. As can be seen in the six insets, the overall profiles of the $R(\omega)$ and $\sigma_1(\omega)$ spectra of the three samples are very similar to each other, especially at high energies above 1000 cm^{-1} . This implies that the doping of Ni only modifies the band structure in a very mild way. It is worth mentioning that the spectra of the pristine $\text{Co}_3\text{Sn}_2\text{S}_2$ are consistent with the earlier reports[29, 30], which demonstrate the following main characters: (1) At low frequencies, the $R(\omega)$ spectra approach to unit at zero frequency and increase as the temperature decreases, indicative of a metallic response. The $\sigma_1(\omega)$ spectra display associated Drude features around zero energy. (2) Two infrared-active phonon signals show up at 160 and 370 cm^{-1} , respectively. (3) The $R(\omega)$ spectra exhibit a

broad absorption structure around 200-300 cm^{-1} , which corresponds to a Lorentz-type peak in the optical conductivity, as denoted by the red arrows in Fig. 1(a) and (d). This peak is thoroughly discussed in previous reports and is ascribed to the interband transition across the inverted band gap close to the Weyl nodes around the E_F [29, 30]. (4) Two Lorentz-type peaks appear at around 1900 and 5000 cm^{-1} , above which the spectra overlap with each other at different temperatures.

Upon doping, the first two of these characters stays almost unchanged. Particularly, the stability of the phonon frequencies indicates that the lattice structure is quite robust against doping. The most remarkable variation is observed at the low energy region, as can be seen in the main panels of Fig. 1. The absorption feature in $R(\omega)$ of the pristine compound obviously weakens in $\text{Co}_{3-x}\text{Ni}_x\text{Sn}_2\text{S}_2$ with $x = 0.11$, and the corresponding Lorentz peak shifts to lower energies, as indicated by the red arrows in the main panels of Fig. 1(b) and (e). The weakening and red shifting of this peak indicate the narrowing of the inverted band gap, which agrees well with theoretical calculations[20]. With further doping of $x = 0.17$, the absorption structure in $R(\omega)$ and the associated Lorentz-type peak are completely out of sight, as can be seen in Fig. 1(c) and (f). There are two possible explanations for these phenomena: one is that the inverted gap is totally closed, and the other one is that the E_F simply moves out of this gap. We will revisit this issue later and discuss it in more detail.

In order to capture the delicate modification of band structure by doping, we use the Drude-Lorentz model to decompose the optical conductivity $\sigma_1(\omega)$. The dielectric function of the Drude-Lorentz model can be expressed as

$$\varepsilon(\omega) = \varepsilon_\infty - \sum_s \frac{\omega_{ps}^2}{\omega^2 + \frac{i\omega}{\tau_{Ds}}} + \sum_j \frac{S_j^2}{\omega_j^2 - \omega^2 - \frac{i\omega}{\tau_j}}.$$

Where ε_∞ is the dielectric constant at high energy; the middle term is the Drude component, which describes the electrodynamics of itinerant carriers; and the last term is the Lorentz component that characterizes the excitation of the energy gap or interband transition. The fitting results of $\sigma_1(\omega)$ at 10 K and 300 K for all three samples are shown in the main panels and insets of Fig. 2(a)-(c), respectively. The specific fitting parameters below 3000 cm^{-1} are shown in Table I. It is worth noting that at room temperature the optical conductivity can be well reproduced by one Drude and one Lorentz term below 3000 cm^{-1} for all three samples. By contrast, the spectra become more complicated and more Drude/Lorentz terms are required at low temperatures.

The pristine $\text{Co}_3\text{Sn}_2\text{S}_2$ compound experiences a ferromagnetic phase transition at $T_C = 175$ K, below which the Drude peak becomes much sharper and extra Lorentz peaks show up in the $\sigma_1(\omega)$ spectra. In previous infrared studies, Yang *et al.* described the emergent feature with

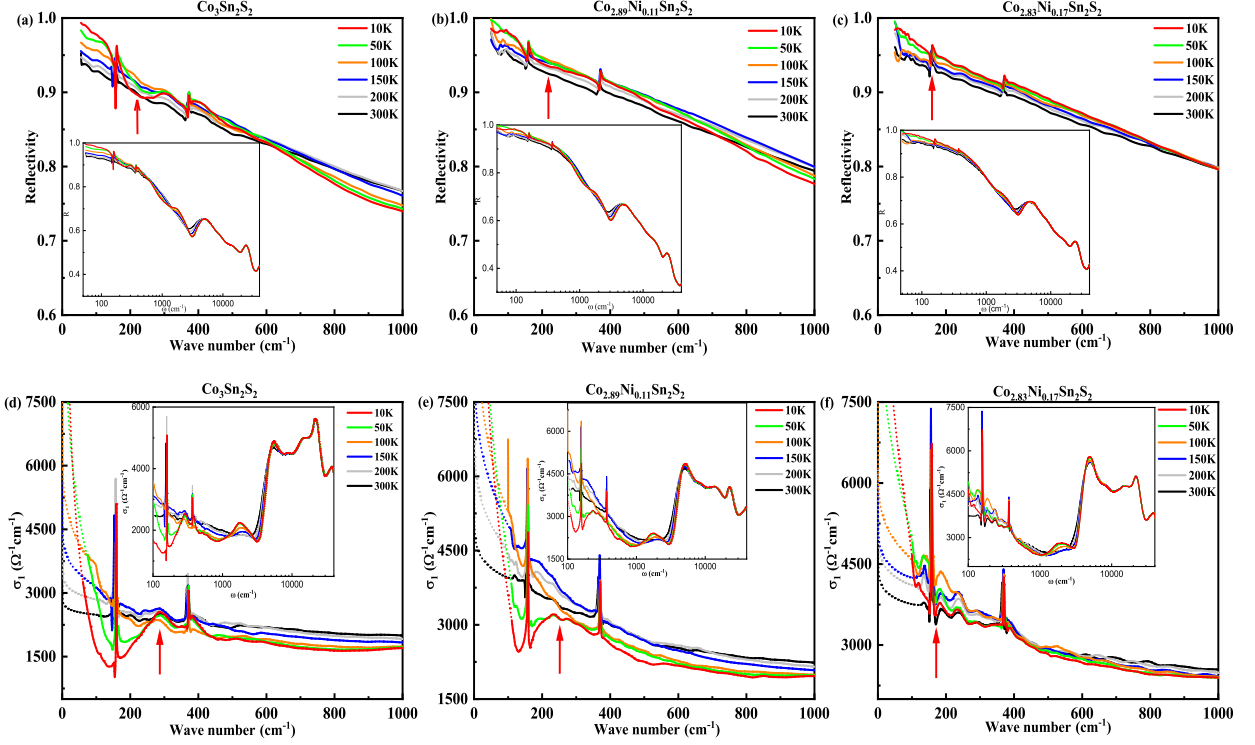


FIG. 1. (a)-(c) Optical reflectivity spectra of $\text{Co}_{3-x}\text{Ni}_x\text{Sn}_2\text{S}_2$ ($x = 0, 0.11$ and 0.17) single crystals at six different temperatures. The insets show the spectra up to $40\,000\text{ cm}^{-1}$. (d)-(f) The real part of optical conductivity $\sigma_1(\omega)$ of $\text{Co}_{3-x}\text{Ni}_x\text{Sn}_2\text{S}_2$ obtained through the Kramers-Kronig transformation. The insets show the expanded $\sigma_1(\omega)$ spectra up to $40\,000\text{ cm}^{-1}$. The extrapolated part through the K-K transformation is represented by the dotted line.

TABLE I. The fitting parameters of $\sigma_1(\omega)$ for three samples below 3000 cm^{-1} for 10 K and 300 K in the unit of cm^{-1} . ω_p is the plasma frequency and $\gamma_D = 1/\tau$ is the scattering rate of free carriers. ω_j , $\gamma_j = 1/\tau_j$, and S_j represent for the resonance frequency, the width, and the square root of the oscillator strength of Lorentz terms, respectively.

x	T	ω_{p1}	γ_{D1}	Lorentz1			Lorentz2			ω_3	γ_3	S_3
				ω_1	γ_1	S_1	ω_2	γ_2	S_2			
$x = 0$	10K	4818	42	316	331	6459	861	1292	8587	1860	1525	11601
	300K	14126	1345							2090	2637	10457
$x = 0.11$	10K	6078	54	252	270	5696	696	1601	11548	1843	1781	11810
	300K	12409	662							2018	4401	18832
$x = 0.17$	10K	4583	38	13413	858					1929	2339	15889
	300K			15082	1013					2066	3007	14293

one Lorentz peak[29], whereas Xu *et al.* suggested multiple Lorentz peaks[30]. Here, we find our data could be well reproduced by two Lorentz peaks, which will be labeled as Lorentz1 and Lorentz2 in the following text. According to previous reports, these two peaks are ascribed to interband transition associated with the inverted band gap close to the Weyl nodes, which locate at 316 cm^{-1} and 861 cm^{-1} at 10 K, respectively. As can be seen from Table I, the Ni doping of $x = 0.11$ causes the shift of Lorentz1 and Lorentz2 to 252 cm^{-1} and 696 cm^{-1} . This infers that the band gap of the interband transition related to the

Weyl nodes is quantitatively reduced. As a result, the integrated Berry curvature is expected to be elevated, and hence leads to the enhancement of the AHE.

With further doping of $x = 0.17$, we find that an additional Drude term is needed to well reproduce the $\sigma_1(\omega)$ at low temperatures, instead of two Lorentz peaks as in $\text{Co}_3\text{Sn}_2\text{S}_2$ and $\text{Co}_{2.89}\text{Ni}_{0.11}\text{Sn}_2\text{S}_2$. It seems that there is a fundamental change to the band structures caused by the excessive amount of Ni doping. As mentioned earlier, one possible scenario is that the inverted energy gaps near the E_F are fully closed. However, considering that

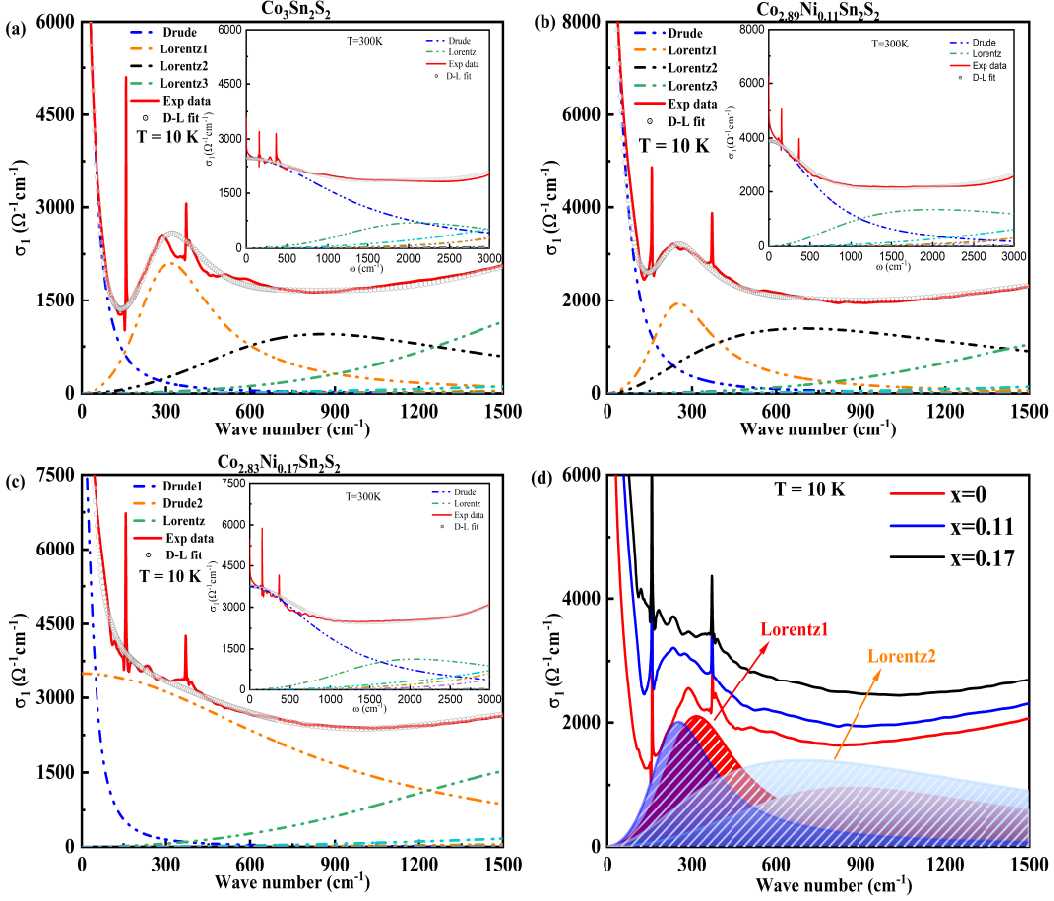


FIG. 2. The Drude-Lorentz fitting of optical conductivity $\sigma_1(\omega)$ at $T = 10\text{ K}$ for (a) $x = 0$, (b) $x = 0.11$, and (c) $x = 0.17$, while the corresponding Drude-Lorentz fitting of $\sigma_1(\omega)$ at $T = 300\text{ K}$ are shown in each inset. (d) Experimental real parts $\sigma_1(\omega)$ at low energies for three samples at $T = 10\text{ K}$. Two peak-like features (Lorentz1 and Lorentz2) in the $\sigma_1(\omega)$ obtained by Drude-Lorentz fitting are present when $x = 0$ and 0.11 , respectively.

neither the lattice structure nor the ferromagnetic phase transition are noticeably modified by doping, we believe that the inverted band gaps will survive as well, which are guaranteed by spin-orbital coupling. Therefore, it is more likely that the E_F shifts out of the inverted band gap and crosses with the initial conduction band. Consequently, some interband transitions disappear from the $\sigma_1(\omega)$ spectra and extra intraband transitions emerge, which agrees perfectly with our results. Moreover, this scenario is also consistent with the theoretical prediction that E_F is pushed upwards upon doping, and the ARPES results that extra electron pocket appears near E_F , occupied by added electrons. In this case, the AHE is not as large as when the E_F is inside the inverted gap.

The low-energy Drude component represents the response of free carriers, which becomes narrower with temperature decreasing for all three samples, showing good metallicity. In order to extract the doping effect, we plot the optical conductivity spectra at 10

K in Fig. 2(d). It is clearly seen that the Drude peak broadens with increasing of the doping level. For $\text{Co}_3\text{Sn}_2\text{S}_2$ and $\text{Co}_{2.89}\text{Ni}_{0.11}\text{Sn}_2\text{S}_2$, the low energy part can be well fitted by only one Drude component, whereas two of them are required to fit the low frequency part of $\text{Co}_{2.83}\text{Ni}_{0.17}\text{Sn}_2\text{S}_2$. The two Drude terms represent free carriers from different Fermi surfaces, one of which gradually emerges below T_C . As shown in Table I, the scattering rate of the first Drude component of $\text{Co}_{2.83}\text{Ni}_{0.17}\text{Sn}_2\text{S}_2$ (38 cm^{-1}) is actually comparable to that of $\text{Co}_3\text{Sn}_2\text{S}_2$ (42 cm^{-1}) and $\text{Co}_{2.89}\text{Ni}_{0.11}\text{Sn}_2\text{S}_2$ (54 cm^{-1}), which infers that the disorder effect on the corresponding conduction band is negligible. Meanwhile, the scattering rate of the second Drude term of $\text{Co}_{2.83}\text{Ni}_{0.17}\text{Sn}_2\text{S}_2$ is much larger, which is absent in $\text{Co}_3\text{Sn}_2\text{S}_2$ and $\text{Co}_{2.89}\text{Ni}_{0.11}\text{Sn}_2\text{S}_2$, hence contributes a large portion of extra itinerant carriers.

The carrier density n can be reflected by the plasma frequency $\omega_p^2 = 4\pi ne^2/m^*$, where m^* is the effective mass

of electrons. The overall plasma frequency for two Drude components can be extracted from $\omega_p = (\omega_{p1}^2 + \omega_{p2}^2)^{1/2}$. As shown in Fig. 3, ω_p of the undoped $\text{Co}_3\text{Sn}_2\text{S}_2$ decreases abruptly by entering the FM phase, due to the opening of energy gaps. Although the FM phase transition is barely affected by doping, this sudden decrease of ω_p becomes less obvious in $\text{Co}_{2.89}\text{Ni}_{0.11}\text{Sn}_2\text{S}_2$ and totally disappears in $\text{Co}_{2.83}\text{Ni}_{0.17}\text{Sn}_2\text{S}_2$, which resembles the evolution of Lorentz1 and Lorentz2. On the other hand, with the increase of Ni concentration, the total plasma frequency at 10 K is substantially enhanced, especially when $x = 0.17$. Assuming m^* is a constant, the carrier density n is supposed to exhibit a similar trend. Note that the Hall effect measurements of $\text{Co}_{3-x}\text{Ni}_x\text{Sn}_2\text{S}_2$ demonstrate that the carrier concentration n first decreases monotonically with Ni doping until $x = 0.15$, then it increases slightly up to $x = 0.17$. The enhancement of the AHE is therefore believed to be accompanied by a decrease in the carrier density[20]. This disagreement could be explained by the technical differences between Hall effect and infrared spectroscopy. It is well known that in multi-band materials with both electron and hole Fermi pockets, the Hall measurement might underestimate the overall carrier density, while infrared spectroscopy generally reflects the contribution from both types of carriers. Therefore, we believe that the overall carrier density n actually increases with doping, which provide a new piece of puzzle toward thoroughly understanding the chemical tuning of AHE.

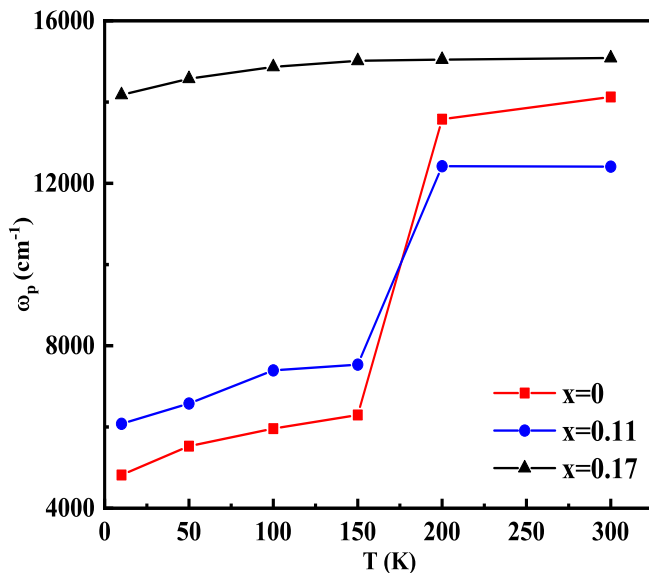


FIG. 3. The temperature-dependent plasma frequency ω_p of $\text{Co}_{3-x}\text{Ni}_x\text{Sn}_2\text{S}_2$ ($x = 0, 0.11$ and 0.17).

At last, we want to discuss the band structure modification induced by doping in a wider energy range. To observe the shift of peaks more clearly, we draw the conductivity spectra of three samples at 10 K in a wide

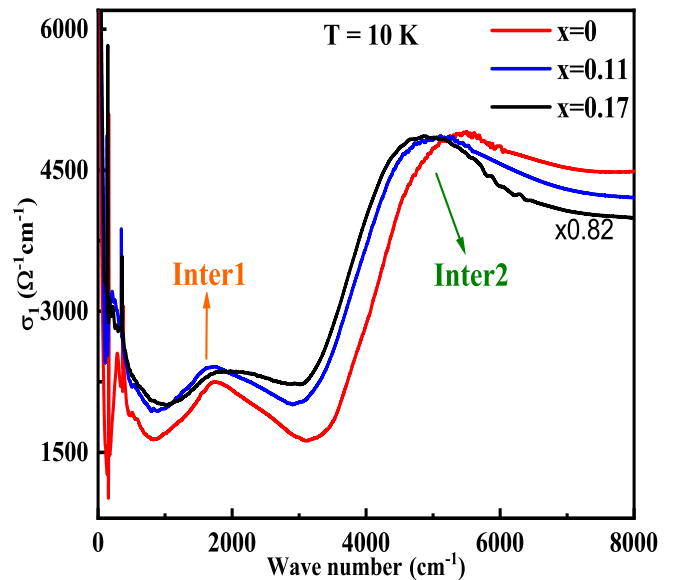


FIG. 4. The real part of optical conductivity $\sigma_1(\omega)$ of $\text{Co}_{3-x}\text{Ni}_x\text{Sn}_2\text{S}_2$ ($x = 0, 0.11$ and 0.17) at 10 K up to 8000 cm^{-1} . For the sake of clarity, y-axis of $\text{Co}_{2.83}\text{Ni}_{0.17}\text{Sn}_2\text{S}_2$ multiplies a scale factor of 0.82.

frequency range up to 8000 cm^{-1} in Fig. 4, where the spectra are shifted vertically for comparison. For the pristine compound, two prominent peaks at around 1900 cm^{-1} and 5000 cm^{-1} could be resolved above 1000 cm^{-1} , which are labeled as Inter1 and Inter2. Inter1 is only noticeable below T_C , and the spectra around the same energies are quite flat at higher temperatures, as shown in Fig. 1(d). Similar behaviors are observed in the doped compounds as well, as seen in Fig. 1(e) and (f), indicating an identical origination. Compared to the undoped compound, Inter1 is almost unchanged at the doping level of $x = 0.11$ at 10 K, but becomes less sharp at $x = 0.17$. This might be caused by the broadening of the associated valence and conduction bands, which is a natural consequence of local disorder effect introduced by doping. Remarkably, band broadening is also believed to be responsible for the narrowing of the inverted band gaps (Lorentz1 and Lorentz2), which is crucial to the enhancement of the AHE[20]. However, the peak position of Inter1 moves slightly to higher energy when the broadening effect is most obvious, which seems to be contradictory to the expected band gap narrowing behavior. This could be explained by the difference between the lowest gap energy and the energy with the most interband transition spectral weight between the valence and conduction bands. The former is determined by the lowest energy of the interband transition peak, whereas the latter one is identified as the central peak position. For Inter1, it is very likely that the corresponding band gap gets smaller upon doping, although the peak position shows a blue shift, due to the redistribution of the joint density of

states.

As for Inter2, the peak position of about 5000 cm^{-1} is smaller than the corresponding theoretical value, which is attributed to the electron correlation by former studies[29, 30]. Moreover, the correlation strength could be estimated by the ratio between peak positions of experimental and theoretical values. Therefore, the peak position of inter2 could serve as a measurement of electron correlation. As can be seen in Fig. 4, Inter2 shifts monotonically to lower energies upon doping, which seems to infer a stronger electron correlation. However, the increase of carrier density by doping usually reduces the correlation strength due to the enhancement of screening effect. Therefore, it is hard to be believed that the increase of electron correlation is responsible for the red-shift of Inter2. In addition, the steepness of the left side of this peak is considered to be related to the correlation strength as well, which almost stays unchanged upon doping. Taking all the above results into consideration, we believe that the doping of Ni has affected the high-energy band structure as well, which causes some of the occupied and unoccupied bands getting closer to each other. More advanced theoretical calculation techniques are required to reveal the exact band structures modified by doping.

CONCLUSION

In summary, we systematically study the optical spectroscopy of $\text{Co}_{3-x}\text{Ni}_x\text{Sn}_2\text{S}_2$ crystals at $x = 0, 0.11$ and 0.17 . We find that the interband transition peaks associated with the inverted energy gaps close to the Weyl nodes get smaller with Ni doping of $x = 0.11$, but disappear completely with $x = 0.17$. Considering that an extra Drude component shows up in the $x = 0.17$ compound, we deduce that the E_F shifts out of the inverted band gap in this system. We also observe the evidence of band broadening, which might be related to the narrowing of the inverted band gap. These results are consistent with previous theoretical calculation, which are essential to the abnormal enhancement of the AHE. On the other hand, the low temperature plasma frequency increases monotonically with the increase of Ni concentration, indicating enhancement of carrier density, which is different from Hall measurement results. In addition, we also discover that interband transition peak at around 5000 cm^{-1} shifts to lower energy upon doping, of which the underlying mechanism is unknown yet. Our results not only provide experimental evidence of band structure modification that is crucial to the enhancement of AHE, but also offer new insights about the chemical tuning of AHE of topological materials.

ACKNOWLEDGEMENTS

This work was supported by the National Key Projects for Research and Development of China (Grant No. 2021YFA1400400, and 2022YFA1403800), and the National Natural Science Foundation of China (Grant No. 12074042), and the Strategic Priority Research Program (B) of the Chinese Academy of Sciences (CAS) (XDB33000000), and the Young Scientists Fund of the National Natural Science Foundation of China (Grant No. 11704033).

* These authors are co-first authors of the article.

† Corresponding authors.

- [1] E. Hall, *Philos. Mag* **12**, 157 (1881).
- [2] A. Kundt, *Wied. Ann* **49**, 257 (1893).
- [3] M. V. Berry, *Proc. Math. Phys. Eng. Sci.* **392**, 45 (1984).
- [4] J. Smit, *Physica* **24**, 39 (1958).
- [5] L. Berger, *Phys. Rev. B* **2**, 4559 (1970).
- [6] T. Jungwirth, Q. Niu, and A. H. MacDonald, *Phys. Rev. Lett.* **88**, 207208 (2002).
- [7] M. Onoda and N. Nagaosa, *J. Phys. Soc. Japan* **71**, 19 (2002).
- [8] F. D. M. Haldane, *Phys. Rev. Lett.* **93**, 206602 (2004).
- [9] N. Nagaosa, J. Sinova, S. Onoda, A. H. MacDonald, and N. P. Ong, *Rev. Mod. Phys.* **82**, 1539 (2010).
- [10] X. Wang and J. Tan, *Appl. Phys. Lett.* **121**, 161903 (2022).
- [11] S. Nakatsuji, N. Kiyohara, and T. Higo, *Nature* **527**, 212 (2015).
- [12] Q. Wang, S. Sun, X. Zhang, F. Pang, and H. Lei, *Phys. Rev. B* **94**, 075135 (2016).
- [13] S. H. Lee, Y. Zhu, Y. Wang, L. Miao, T. Pillsbury, H. Yi, S. Kempinger, J. Hu, C. A. Heikes, P. Quarterman, W. Ratcliff, J. A. Borchers, H. Zhang, X. Ke, D. Graf, N. Alem, C.-Z. Chang, N. Samarth, and Z. Mao, *Phys. Rev. Res.* **1**, 012011 (2019).
- [14] A. A. Burkov, M. D. Hook, and L. Balents, *Phys. Rev. B* **84**, 235126 (2011).
- [15] Z. Fang, N. Nagaosa, K. S. Takahashi, A. Asamitsu, R. Mathieu, T. Ogasawara, H. Yamada, M. Kawasaki, Y. Tokura, and K. Terakura, *Science* **302**, 92 (2003).
- [16] A. A. Burkov, *Phys. Rev. Lett.* **113**, 187202 (2014).
- [17] P. V. C. Medeiros, S. Stafström, and J. Björk, *Phys. Rev. B* **89**, 041407 (2014).
- [18] E. Liu, Y. Sun, N. Kumar, L. Muechler, A. Sun, L. Jiao, S.-Y. Yang, D. Liu, A. Liang, Q. Xu, *et al.*, *Nat. Phys* **14**, 1125 (2018).
- [19] Q. Wang, Y. Xu, R. Lou, Z. Liu, M. Li, Y. Huang, D. Shen, H. Weng, S. Wang, and H. Lei, *Nat. Commun* **9**, 1 (2018).
- [20] J. Shen, Q. Yao, Q. Zeng, H. Sun, X. Xi, G. Wu, W. Wang, B. Shen, Q. Liu, and E. Liu, *Phys. Rev. Lett.* **125**, 086602 (2020).
- [21] J. Shen, Q. Zeng, S. Zhang, H. Sun, Q. Yao, X. Xi, W. Wang, G. Wu, B. Shen, Q. Liu, and E. Liu, *Adv. Funct. Mater.* **30**, 2000830 (2020).
- [22] J. Liu, L. Ding, L. Xu, X. Li, K. Behnia, and Z. Zhu, *J. Phys. Condens. Matter* **35**, 375501 (2023).

- [23] H. Zhou, G. Chang, G. Wang, X. Gui, X. Xu, J.-X. Yin, Z. Guguchia, S. S. Zhang, T.-R. Chang, H. Lin, W. Xie, M. Z. Hasan, and S. Jia, [Phys. Rev. B](#) **101**, 125121 (2020).
- [24] G. S. Thakur, P. Vir, S. N. Guin, C. Shekhar, R. Wehrich, Y. Sun, N. Kumar, and C. Felser, [Chem. Mater.](#) **32**, 1612 (2020).
- [25] H. Iohani, P. Foulquier, P. Le Fèvre, F. m. c. Bertran, D. Colson, A. Forget, and V. Brouet, [Phys. Rev. B](#) **107**, 245119 (2023).
- [26] M. Dressel, G. Gruener, and G. F. Bertsch, [Am J Phys](#) **70**, 1269 (2002).
- [27] C. C. Homes, M. Reedyk, D. Cradles, and T. Timusk, [Appl. Opt](#) **32**, 2976 (1993).
- [28] D. B. Tanner, [Phys. Rev. B](#) **91**, 035123 (2015).
- [29] R. Yang, T. Zhang, L. Zhou, Y. Dai, Z. Liao, H. Weng, and X. Qiu, [Phys. Rev. Lett.](#) **124**, 077403 (2020).
- [30] Y. Xu, J. Zhao, C. Yi, Q. Wang, Q. Yin, Y. Wang, X. Hu, L. Wang, E. Liu, G. Xu, *et al.*, [Nat. Commun](#) **11**, 1 (2020).